PAPER

# Optical conductivity in an effective model for graphene: finite temperature corrections

IOP Publishing Journal of Physics A: Mathematical and Theoretical
J. Phys. A: Math. Theor. **53** (2020) 015401 (21pp) https://doi.org/10.1088/1751-8121/ab57cb

# Optical conductivity in an effective model for graphene: finite temperature corrections

**Horacio Falomir[1], Enrique Muñoz[2,3], Marcelo Loewe[2,4,5] and Renato Zamora[6,7]**

[1] Facultad de Ciencias Exactas de la UNLP, IFLP, CONICET—Departamento de Física, C.C. 67, (1900) La Plata, Argentina
[2] Instituto de Física, Pontificia Universidad Católica de Chile, Avenida Vicuña Mackenna 4860, Santiago, Chile
[3] Center for Nanotechnology and Advanced Materials CIEN-UC, Avenida Vicuña Mackenna 4860, Santiago, Chile
[4] Centre for Theoretical and Mathematical Physics, University of Cape Town, Rondebosch 770, South Africa
[5] Centro Científico Tecnológico de Valparaíso, CCTVAL, Universidad Técnica Federico Santa María, Casilla 110-V, Valparaíso, Chile
[6] Instituto de Ciencias Básicas, Universidad Diego Portales, Casilla 298-V, Santiago, Chile
[7] Centro de Investigación y Desarrollo de Ciencias Aeroespaciales (CIDCA), Fuerza Aérea de Chile, Santiago 8020744, Chile

E-mail: falomir@fisica.unlp.edu.ar, munozt@fis.puc.cl, mloewe@fis.puc.cl and rzamorajofre@gmail.com

Received 19 July 2019, revised 12 October 2019
Accepted for publication 14 November 2019
Published 3 December 2019


**Abstract**

In this article, we investigate the temperature and chemical potential dependence of the optical conductivity of graphene, within a field theoretical representation in the continuum approximation, arising from an underlying tight-binding atomistic model, that includes up to second-nearest neighbors coupling. Our calculations allow us to obtain the dependence of the optical conductivity on frequency, temperature and finite chemical potential, thus generalizing our previously reported calculations at zero temperature, and reproducing the universal and experimentally verified value at zero frequency. Moreover, we also show that a small but still measurable shift in the conductance minimum arises as a function of the second-nearest neighbors hopping $t'$, thus providing the possibility to directly measure this parameter in transport experiments.

  

Keywords: optical conductivity, graphene, Matsubara formalism, thermal field theory, finite temperature

(Some figures may appear in colour only in the online journal)

## 1. Introduction

Graphene, a monolayer of carbon atoms arranged in a honeycomb lattice with $C_{3v} \otimes Z_2$ symmetry [1], possesses an electronic spectrum that displays two non-equivalent points $K_+$, $K_-$ where the conduction and valence bands touch, and in whose vicinity the dispersion relation is approximately linear. The electronic spectrum is correctly described by an atomistic tight-binding model that, when including up to first-nearest neighbors coupling, leads to an effective low-energy continuum model describing relativistic Dirac fermions in 2D. Transparency is a physical property determined by the optical conductivity, i.e. the linear response to an external electromagnetic field. Several experiments confirm [3–16] that the measured transmittance is indeed compatible with the effective single-particle model of relativistic Dirac fermions in graphene, as supported by a large number of theoretical works [8–16, 18–21]. Moreover, the frequency-dependence of the conductivity in graphene, whithin this effective Dirac theory arising from first-nearest neighbors approximation, has been calculated at finite temperature and chemical potential [21], including the effect of scattering by impurities [20, 21] as well as many-body screening due to polarization [18, 19].

Several many-body effects may induce deviations from the single-particle Dirac dispersion continuum model, such as electron–electron Coulomb interactions [17, 22], lattice phonons [23–27], impurities [20, 21, 28–30] and different forms of quenched disorder [17, 30]. Nevertheless, at the fundamental level of the atomistic single-particle Hamiltonian, the minimal tight-binding model can be extended to include second-nearest neighbors couplings, that in the continuum representation leads to an effective field theory with a quadratic contribution to the linear Dirac dispersion [2]. In this article, we shall focus on the contribution to the optical conductivity that arises in the context of this effective field theory for graphene [31], at finite temperature and chemical potential. Such a model has been considered by some of us in [2] to fully account for the anomalous integer quantum Hall effect in this material and the underlying wave equation is referred to in literature as second order Dirac equation [32]. Notice that this is an isotropic model in which, the quadratic (anisotropic next to leading) term in the dispersion relation coming from the first-nearest neighbor sites has been shown to give a vanishing contribution to the Hamiltonian spectrum at first order in perturbation theory, thus justifying the consideration of the quadratic (isotropic) leading contribution of second-nearest neighbors in the honeycomb array [2]. In a previous article [31], we investigated the frequency dependence of the zero-temperature optical conductivity of graphene, calculated in the Kubo linear response approximation [33–35], when these second-nearest neighbors corrections are included in an effective field theory on the closed time path (CTP) (or Keldysh [35, 36]) formalism. In our present article, we extend this analysis to include finite temperature and finite chemical potential effects. Along the previously exposed ideas, we have organized the remaining of this article as follows: in section 2, we present the details of the model. In section 3 we present the Matsubara formalism to calculate the vacuum polarization tensor in the Euclidean representation, to finally obtain the optical conductivity from the vacuum polarization tensor via analytic continuation to real frequency space. Our analytical results are summarized by equations (3.21) and (3.27) for the real and imaginary parts of the conductivity, respectively. We discuss our findings in section 4, showing that the explicit dependence of the real part

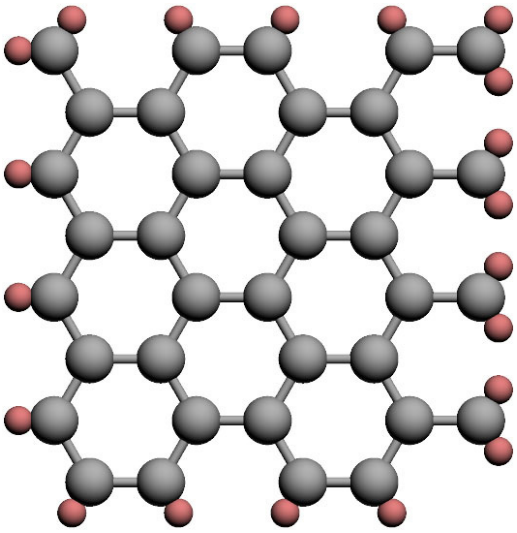

**Figure 1.** Sketch of the crystal structure of graphene. The honeycomb array is described in terms of two overlapping triangular sublattices.

of the conductivity, as displayed in our equation (3.21), could be used in combination with transport experiments to determine the second-nearest neighbor hopping parameter $t'$, whose precise value remains elusive in the current literature [30]. Some calculation details are presented in two appendices.

## 2. Lagrangian, conserved current and generating functional

Graphene crystal structure, as sketched in figure 1, is described in terms of two overlapping triangular (Bravais) sublattices. The band structure obtained from an atomistic, tight-binding description including up to the next-to-nearest neighbors contribution is of the form

$$E_{\pm}(\mathbf{k}) = \pm t\sqrt{f(\mathbf{k})} - t'[f(\mathbf{k}) - 3], \tag{2.1}$$

where $t$ and $t'$ are the nearest and next-to-nearest hopping parameters and

$$f(\mathbf{k}) = 3 + 4\cos\left(\frac{3k_x a}{2}\right)\cos\left(\frac{\sqrt{3}k_y a}{2}\right) + 2\cos(\sqrt{3}k_y a). \tag{2.2}$$

Here, $a \simeq 1.42$ Å is the interatomic distance [30]. The literature reports a value [30] $t \sim 2.8$ eV, while for the second nearest-neighbour coupling the reference values are not so precisely established, but reported in the range [30] $0.02t \leqslant t' \leqslant 0.2t$.

The points $K_+$ and $K_-$ at which $f(K_\pm) = 0$ define the so-called Dirac points. Around $K_+$,

$$E_{\pm}(\mathbf{k} + K_+) = \pm t\left[\frac{3}{2}a|\mathbf{k}| - \frac{3}{8}a^2\mathbf{k}^2\sin(3\vartheta)\right] + t'\left[-\frac{9}{4}a^3\mathbf{k}^2 + 3\right] + \mathcal{O}(|\mathbf{k}|^3), \tag{2.3}$$

with $\tan(\vartheta) = k_y/k_x$. Around the $K_-$ point, one just needs to replace $\vartheta \to -\vartheta$ in equation (2.3). The isotropic portion of the model in equation (2.3) was first considered in [2] as a natural framework to explain the anomalous integer quantum Hall effect in graphene. Moreover, as previously mentioned, the anisotropic quadratic term, so called trigonal warping,

**Table 1.** Parameters of the model.

| | |
|---|---|
| $a$ (Å) [30] | 1.42 |
| $t$ (eV) [30] | 2.8 |
| $t'$ (eV) [30] | ∼0.056–0.56 |
| $m$ (kg) | $1.37\times10^{-29}$–$1.37\times10^{-30}$ |
| $v_f$ (m s$^{-1}$) [30] | $\sim10^6$ |
| $mv_f^2$ (eV) | 7–70 |

in this effective dispersion relation was shown not to contribute to the energy spectrum at first order in perturbation theory [2], thus justifying to retain just the isotropic terms up to this order in the pseudo-momenta.

In the presence of electromagnetic interactions, the model in the continuum approximation is described by an effective field theory with the Lagrangian [2, 31]

$$\begin{aligned}\mathcal{L} :=& \frac{\mathrm{i}}{2}\left[\psi^\dagger\,\partial_t\psi-\partial_t\psi^\dagger\,\psi\right]+\psi^\dagger eA_0\psi\\ &-\frac{1}{2m}\left\{\left[\left(\mathbf{p}-e\mathbf{A}+\theta\boldsymbol{\sigma}\right)\psi\right]^\dagger\cdot\left[\left(\mathbf{p}-e\mathbf{A}+\theta\boldsymbol{\sigma}\right)\psi\right]-2\theta^2\psi^\dagger\psi\right\}\\ =&\frac{\mathrm{i}}{2}\left[\psi^\dagger\,\partial_t\psi-\partial_t\psi^\dagger\,\psi\right]-\frac{1}{2m}\left\{\boldsymbol{\nabla}\psi^\dagger\cdot\boldsymbol{\nabla}\psi+\mathrm{i}\boldsymbol{\nabla}\psi^\dagger\cdot\left(-e\mathbf{A}+\theta\boldsymbol{\sigma}\right)\psi\right.\\ &\left.-\mathrm{i}\psi^\dagger\left(-e\mathbf{A}+\theta\boldsymbol{\sigma}\right)\cdot\boldsymbol{\nabla}\psi+\psi^\dagger\left[\left(-e\mathbf{A}+\theta\boldsymbol{\sigma}\right)^2-2\theta^2\right]\psi\right\},\end{aligned}\tag{2.4}$$

where $\theta=mv_{\mathrm{F}}$ and $m=\pm2\hbar^2/(9t'a^2)$, where the sign depends on each Dirac cone $K_\pm$. The gauge invariance of this Lagrangian was discussed in detail in our previous work [2, 31].

A summary of the numerical values for the relevant parameters of the model is presented in table 1.

Here, the three-momentum is $p^\mu=(p^0,\mathbf{p})$, with $\mathbf{p}=(p^1,p^2)$. The vector potential $\mathbf{A}=(A^1,A^2)$, whereas $\boldsymbol{\sigma}=(\sigma^1,\sigma^2)$ are Pauli matrices. In this model, $\psi^\dagger$ and $\psi$ are regarded as independent fields whose equations of motion are derived from the variation of the action,

$$\begin{aligned}\frac{\partial\mathcal{L}}{\partial\psi^\dagger}-\partial_t\left(\frac{\partial\mathcal{L}}{\partial\left(\partial_t\psi^\dagger\right)}\right)-\boldsymbol{\nabla}\cdot\left(\frac{\partial\mathcal{L}}{\partial\left(\boldsymbol{\nabla}\psi^\dagger\right)}\right)&\\ =\mathrm{i}\partial_t\psi-\frac{1}{2m}\left[\left(\mathbf{p}-e\mathbf{A}+\theta\boldsymbol{\sigma}\right)^2-2\theta^2\right]\psi=0,&\end{aligned}\tag{2.5}$$

and similarly for $\psi$.

Nœther's theorem leads to the existence of a locally conserved current, whose time-component defines the local charge density [31]

$$j^0=e\,\psi^\dagger\psi,\tag{2.6}$$

while the spatial components define the current density [31]

$$j^k=\frac{e}{2m}\left\{\mathrm{i}\left(\partial^k\psi^\dagger\,\psi-\psi^\dagger\,\partial^k\psi\right)+2\psi^\dagger\left(-eA^k+\theta\sigma^k\right)\psi\right\}.\tag{2.7}$$

It is straightforward to verify, from the equations of motion, that $j^\mu$ is conserved [31],

$$\partial_\mu j^\mu=\partial_t j^0-\boldsymbol{\nabla}\cdot\mathbf{j}=0.\tag{2.8}$$

Notice also that we can write [31]

$$j^{\mu}(x) = \frac{\delta}{\delta A_{\mu}(x)} \int \mathcal{L}(y)\, \mathrm{d}^3 y. \tag{2.9}$$

In our previous work [31], we developed a generating functional on the CTP (or Keldysh contour) for the effective field theory in equation (2.3), defined as

$$Z_{\gamma}[A] = \int \mathcal{D}\psi^{\dagger}(\mathbf{x},\tau)\mathcal{D}\psi(\mathbf{x},\tau)\mathrm{e}^{\mathrm{i}\int_{\gamma}\mathrm{d}\tau\int \mathrm{d}^2\mathbf{x}\mathcal{L}[\psi^{\dagger}(\mathbf{x},\tau),\psi(\mathbf{x},\tau)]}, \tag{2.10}$$

with $\gamma = \gamma_{-} \oplus \gamma_{+}$, such that $\gamma_{-}$ represents the time-ordered branch of the contour, while $\gamma_{+}$ is the anti-time-ordered branch (see [31] for details). From the CTP functional defined in equation (2.10), we generate the average current components as follows [31]

$$\begin{aligned} -\mathrm{i}\frac{\delta \log Z_{\gamma}[A]}{\delta A_{\mu}(x)} &= \frac{1}{Z_{\gamma}[A]} \int \mathcal{D}\psi^{\dagger}\mathcal{D}\psi\, \mathrm{e}^{\mathrm{i}\int_{\gamma}\mathrm{d}^3 y \mathcal{L}(y)} j^{\mu}(x) \\ &= \langle j^{\mu}(x)\rangle\,, \end{aligned} \tag{2.11}$$

while the second functional derivative gives the current-current correlation function [31],

$$\begin{aligned} (-\mathrm{i})^2 \frac{\delta^2 \log Z_{\gamma}[A]}{\delta A_{\mu}(x)\delta A_{\nu}(y)} &= -\mathrm{i}\left\langle \frac{\delta j^{\mu}(x)}{\delta A_{\nu}(y)} \right\rangle + \langle \mathcal{T} j^{\mu}(x) j^{\nu}(y)\rangle \\ &\quad - \langle j^{\mu}(x)\rangle \langle j^{\nu}(y)\rangle\,. \end{aligned} \tag{2.12}$$

Here, the first term is the *diamagnetic contribution* [31, 37]

$$\left\langle \frac{\delta j^{\mu}(x)}{\delta A_{\nu}(y)} \right\rangle = \delta^{\mu k}\delta^{\nu}_{k}\left(-\frac{e^2}{m^2}\right)\langle \psi^{\dagger}(x)\psi(x)\rangle\, \delta^{(3)}(x-y)\,, \tag{2.13}$$

and the others are the *paramagnetic* ones.

The currents are defined in normal order with respect to the fermionic field, so that $\langle j^{\mu}(x)\rangle|_{A=0} = 0$. The linear response of the system to the external electromagnetic field is described by the second derivative in equation (2.12) evaluated at $A_{\mu} = 0$ [31, 37],

$$\begin{aligned} K^{\mu\nu}(x,y) &= (-\mathrm{i})^2 \frac{\delta^2 \log Z_{\gamma}[A]}{\delta A_{\mu}(x)\delta A_{\nu}(y)}\bigg|_{A=0} = K^{\nu\mu}(y,x) \\ &= \langle \mathcal{T} j^{\mu}(x) j^{\nu}(y)\rangle_0\,. \end{aligned} \tag{2.14}$$

The spatial components of the current are given by [31]

$$\begin{aligned} j^{k}(x)\Big|_{A=0} &= \frac{e}{2m}\left\{\mathrm{i}\partial^{k}\psi^{\dagger}(x)\psi(x) - \mathrm{i}\psi^{\dagger}(x)\partial^{k}\psi(x) + 2\theta\psi^{\dagger}(x)\sigma^{k}\psi(x)\right\} \\ &\equiv \psi^{\dagger}_{a}(x)\hat{D}^{k}_{ab}\psi_{b}(x), \end{aligned} \tag{2.15}$$

where we have defined the differential operators [31]

$$\hat{D}^{k}_{ab} = \frac{e}{2m}\left\{-\mathrm{i}\overset{\leftrightarrow}{\partial^{k}}\delta_{ab} + 2\theta\left[\sigma^{k}\right]_{ab}\right\}. \tag{2.16}$$

Applying Wick's theorem [35, 36, 38] on the CTP for the definition of the current-correlator (correlators associated to disconnected diagrams vanish), we obtain [31]:

$$\begin{aligned}\langle \mathcal{T} j^k(x) j^l(y)\rangle &= \langle \mathcal{T}\psi_a^\dagger(x)\hat{D}^k_{ab}\psi_b(x)\psi_c^\dagger(y)\hat{D}^l_{cd}\psi_d(y)\rangle \\ &= -\hat{D}^k_{ab}\hat{D}^l_{cd}\langle \mathcal{T}\psi_b(x)\psi_c^\dagger(y)\rangle\langle \mathcal{T}\psi_d(y)\psi_a^\dagger(x)\rangle.\end{aligned} \tag{2.17}$$

The previous relation allows us to define the corresponding components of the polarization tensor in the CTP contour indices $\alpha, \beta = \pm$,

$$\begin{aligned}K^{kl}_{\alpha\beta}(x,y) &= \langle \mathcal{T} j^k_\alpha(x) j^l_\beta(y)\rangle \\ &= -\hat{D}^k_{ab}\hat{D}^l_{cd}\Delta^{\alpha\beta}_{bc}(x,y)\Delta^{\beta\alpha}_{da}(y,x).\end{aligned} \tag{2.18}$$

As discussed in detail in [31], the retarded component of the polarization tensor is obtained from the combination

$$\begin{aligned}K^{kl}_R(x,y) &= K^{kl}_{--}(x,y) - K^{kl}_{-+}(x,y) \\ &= \hat{D}^k_{ab}\hat{D}^l_{cd}\Big\{\Delta^{\rm F}_{bc}(x,y)\Delta^A_{da}(y,x) + \Delta^R_{bc}(x,y)\Delta^{\rm F}_{da}(y,x) \\ &\quad - \Delta^R_{bc}(x,y)\Delta^A_{da}(y,x)\Big\}.\end{aligned} \tag{2.19}$$

In terms of Fourier transforms,

$$\psi(x) = \frac{1}{(2\pi)^{3/2}}\int \mathrm{d}^3p\, \mathrm{e}^{-\mathrm{i}p\cdot x}\tilde{\psi}(p), \qquad \psi^\dagger(x) = \frac{1}{(2\pi)^{3/2}}\int \mathrm{d}^3p\, \mathrm{e}^{\mathrm{i}p\cdot x}\tilde{\psi}^\dagger(p), \tag{2.20}$$

we have [31]

$$\Delta^{\alpha\beta}_{ab}(x,y) \equiv \Delta^{\alpha\beta}_{ab}(x-y) = \int \frac{\mathrm{d}^3p}{(2\pi)^3}\mathrm{e}^{\mathrm{i}(x-y)\cdot p}\tilde{\Delta}^{\alpha\beta}_{ab}(p). \tag{2.21}$$

Here, the different propagators for the Hamiltonian model considered are, in Fourier space (F: Feynman, R: Retarded, A: Advanced),

$$\begin{aligned}\tilde{\Delta}^{\rm F}(p) = \tilde{\Delta}_{--}(p) &= \mathrm{i}\frac{p_0 - \frac{\mathbf{p}^2}{2m} + v_{\rm F}\mathbf{p}\cdot\boldsymbol{\sigma}}{\left(p_0 - \frac{\mathbf{p}^2}{2m}\right)^2 - v_{\rm F}^2\mathbf{p}^2 + \mathrm{i}\epsilon'} \\ &= \mathrm{i}\frac{p_0 - \frac{\mathbf{p}^2}{2m} + v_{\rm F}\mathbf{p}\cdot\boldsymbol{\sigma}}{\left(p_0 + \mathrm{i}\epsilon - \frac{\mathbf{p}^2}{2m} - v_{\rm F}|\mathbf{p}|\right)\left(p_0 - \mathrm{i}\epsilon - \frac{\mathbf{p}^2}{2m} + v_{\rm F}|\mathbf{p}|\right)},\end{aligned} \tag{2.22}$$

$$\tilde{\Delta}^R(p) = \mathrm{i}\frac{p_0 - \frac{\mathbf{p}^2}{2m} + v_{\rm F}\mathbf{p}\cdot\boldsymbol{\sigma}}{\left(p_0 + \mathrm{i}\epsilon - \frac{\mathbf{p}^2}{2m}\right)^2 - v_{\rm F}^2\mathbf{p}^2}, \tag{2.23}$$

$$\tilde{\Delta}^A(p) = \mathrm{i}\frac{p_0 - \frac{\mathbf{p}^2}{2m} + v_{\rm F}\mathbf{p}\cdot\boldsymbol{\sigma}}{\left(p_0 - \mathrm{i}\epsilon - \frac{\mathbf{p}^2}{2m}\right)^2 - v_{\rm F}^2\mathbf{p}^2}. \tag{2.24}$$

In order to consider the finite temperature dependence of the polarization tensor, the time-domain is compactified according to the prescription $t \to -\mathrm{i}\tau$, with $0 \leqslant \tau \leqslant \beta$, with $\beta = 1/(k_{\rm B}T)$ the inverse temperature. Correspondingly, the three propagators defined above

reduce to a single Euclidean one, by analytic continuation $p_0 + \mathrm{i}\epsilon \to \mathrm{i}p_4 + \mu$ of the retarded one. Therefore, we define the Euclidean propagator by

$$\tilde{\Delta}^E(p) = \tilde{\Delta}^R(p_0 + \mathrm{i}\epsilon \to \mathrm{i}p_4 + \mu, \mathbf{p}) = \mathrm{i}\frac{\mathrm{i}p_4 + \mu - \frac{\mathbf{p}^2}{2m} + v_F \mathbf{p}\cdot\boldsymbol{\sigma}}{\left(\mathrm{i}p_4 + \mu - \frac{\mathbf{p}^2}{2m}\right)^2 - v_F^2\mathbf{p}^2}. \tag{2.25}$$

In particular, for the linear response theory [34–36, 38–40], we need the retarded component of the polarization tensor

$$K_R^{\mu\nu}(x-y) = \int \frac{\mathrm{d}^3 p}{(2\pi)^3} \mathrm{e}^{\mathrm{i}(x-y)\cdot p}\, \Pi_R^{\mu\nu}(p), \tag{2.26}$$

which is obtained at finite temperature from the Euclidean polarization tensor by analytic continuation

$$\Pi_R^{kl}(\omega, \mathbf{p}) = \Pi_E^{kl}(\mathrm{i}p_4 \to \omega + \mathrm{i}\epsilon, \mathbf{p}). \tag{2.27}$$

The corresponding expression for the finite temperature, Euclidean polarization tensor is

$$\Pi_E^{kl}(ip_4, \mathbf{p}) = \frac{e^2}{4m^2}\frac{1}{\beta}\sum_{q_4=\omega_n, n\in Z}\int \frac{\mathrm{d}^2 q}{(2\pi)^2}\Gamma_{ab}^k(p+2q) \times \tilde{\Delta}_{bc}^E(p+q)\Gamma_{cd}^l(p+2q)\tilde{\Delta}_{da}^E(q) \tag{2.28}$$

with the symbol

$$\Gamma_{ab}^k(p+2q) = \left[\delta_{ab}(p+2q)^k + 2\theta\left[\sigma^k\right]_{ab}\right], \tag{2.29}$$

and a similar expression for $\Gamma_{cd}^l(p+2q)$. We remark that due to compactification of the time domain at finite temperature, the component $q_4 = \omega_n$, where $\omega_n = 2\pi(n+1/2)/\beta$ for $n \in \mathbb{Z}$ are the Fermionic Matsubara frequencies.

## 3. The polarization tensor and optical conductivity

The polarization tensor $\Pi^{kl}(p)$ contains the information about the conductivity on the plane of this two-dimensional system and also about its light transmission properties [10, 37]. We are interested in the consequences of the application of harmonic homogeneous electric fields which, in the temporal gauge, are related with the vector potential by $E^k = -\partial A^k/\partial t = -\mathrm{i}\omega A^k$. Since the conductivity is determined by the linear relation between the current and the applied electric field, $J_k = \sigma_{kl}E^l$, from equations (2.11), (2.14) and (2.27), we can write for the conductivity as a function of the frequency [10, 37]

$$\sigma_{kl}(\omega) = 2\times 2\left.\frac{\Pi_{kl}^R(p)}{\mathrm{i}\omega}\right|_{p\to(\omega,\mathbf{0})}, \tag{3.1}$$

where the prefactor takes into account the valley and electronic spin degeneracy in graphene. Therefore, the real and imaginary components of the optical conductivity are given by

$$\Re e\,\sigma_{kl}(\omega, T) = 4\frac{\Im m\,\Pi_{kl}^R(\omega, T)}{\omega} \tag{3.2}$$

and

$$\Im m\,\sigma_{kl}(\omega,T)=-4\frac{\Re e\,\Pi^R_{kl}(\omega,T)}{\omega}, \tag{3.3}$$

respectively. In particular, it is the real part of the conductivity tensor that determines electronic transport in the DC limit $\omega\to 0$.

In order to include finite temperature effects, we first calculate $\Pi^E_{kl}(\omega,\mathbf{0})$ from equation (2.28), and then by analytic continuation, as described in equation (2.27), we obtain $\Pi^R_{kl}(\omega,\mathbf{0})$.

The evaluation requires to calculate two integrals and an infinite sum over (Fermionic) Matsubara frequencies, as defined in equation (2.28).

$$\begin{aligned}\Pi^E_{kl}(p)=\frac{e^2}{4m^2}\frac{1}{\beta}\sum_{q_4=\omega_n,n\in Z}\int\frac{\mathrm{d}^2q}{(2\pi)^2}\mathrm{Tr}\left\{[p_k+2q_k+2\theta\sigma_k]\,\Delta^E(p+q)\right.\\ \left.\times\,[p_l+2q_l+2\theta\sigma_l]\,\Delta^E(q)\right\}.\end{aligned} \tag{3.4}$$

Specializing this expression to the case $p=(\mathrm{i}p_4,\mathbf{0})$, and using polar coordinates for the spatial components $q_1=Q\cos\varphi, q_2=Q\sin\varphi$, we write

$$\Pi^E_{kl}(\mathrm{i}p_4,\mathbf{0})=\frac{e^2}{4\pi}\frac{1}{\beta}\sum_{q_4=\omega_n,n\in Z}\int_0^\infty\frac{\mathrm{d}Q\,Q}{4\pi m^2}\int_0^{2\pi}\mathrm{d}\varphi\frac{\mathrm{Tr}\{A\}}{B^{EE}} \tag{3.5}$$

with

$$\begin{aligned}A&=[2q_k+2\theta\sigma_k]\left[\mathrm{i}p_4+\mathrm{i}q_4+\mu-\frac{\mathbf{q}^2}{2m}+v_\mathrm{F}\mathbf{q}\cdot\boldsymbol{\sigma}\right][2q_l+2\theta\sigma_l]\\ &\quad\times\left[\mathrm{i}q_4+\mu-\frac{\mathbf{q}^2}{2m}+v_\mathrm{F}\mathbf{q}\cdot\boldsymbol{\sigma}\right],\\ B^{EE}&=\left(\left(\mathrm{i}p_4+\mathrm{i}q_4+\mu-\frac{\mathbf{q}^2}{2m}\right)^2-v_\mathrm{F}^2\mathbf{q}^2\right)\left(\left(\mathrm{i}q_4+\mu-\frac{\mathbf{q}^2}{2m}\right)^2-v_\mathrm{F}^2\mathbf{q}^2\right).\end{aligned} \tag{3.6}$$

We notice that the denominator is independent of $\varphi$, and hence it is straightforward to calculate the trace in the numerator integrated over $\varphi$,

$$\begin{aligned}N(Q,\mathrm{i}p_4,\mathrm{i}q_4+\mu)&=\frac{1}{4\pi m^2}\int_0^{2\pi}\mathrm{Tr}\,\{A\}\,\mathrm{d}\varphi\\ &=-\left(8\left(8m^4v_f^2(\mathrm{i}q_4+\mu)(\mathrm{i}q_4+\mu+\mathrm{i}p_4)+4m^2Q^2\right.\right.\\ &\quad\times\left(\mathrm{i}p_4\left(mv_f^2+\mathrm{i}q_4+\mu\right)+(\mathrm{i}q_4+\mu)\left(\mathrm{i}q_4+\mu+2mv_f^2\right)\right))\\ &\quad\left.-2mQ^4\left(mv_f^2+2\mathrm{i}q_4+2\mu+\mathrm{i}p_4\right)+Q^6\right)\end{aligned} \tag{3.7}$$

for $k,l=1,1$ or $2,2$, and a vanishing result for $k,l=1,2$ or $2,1$.

Let us now consider the sum over (Fermionic) Matsubara frequencies, since $q_4=\omega_n=(2n+1)\pi/\beta$. The sum can be obtained through the construction of a contour integral on the complex plane (see figure 2), by choosing a meromorphic function with infinitely many poles at the Matsubara frequencies. A straightforward choice is the Fermi function,

$$n_\mathrm{F}(k_0-\mu)=\frac{1}{1+\mathrm{e}^{\beta(k_0-\mu)}}, \tag{3.8}$$

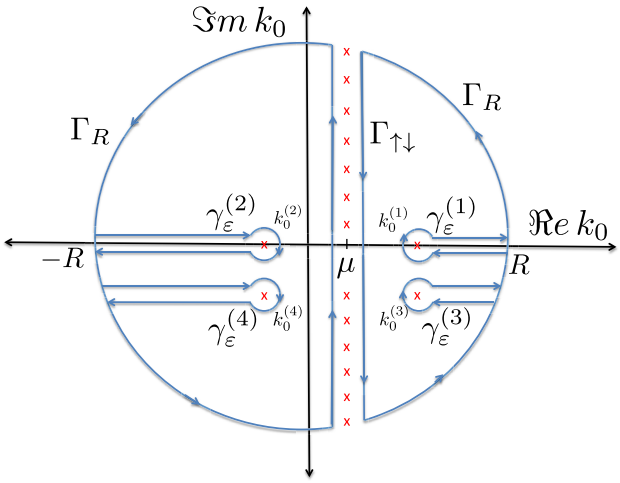


**Figure 2.** The complex contour $C = \Gamma_R \oplus \Gamma_{\uparrow\downarrow} \oplus_\alpha \gamma_\varepsilon^{(\alpha)}$ used to calculate the Matsubara sum. Notice that $\Gamma_{\uparrow\downarrow}$ and $\gamma_\varepsilon^{(\alpha)}$ are oriented clockwise, in order to exclude the poles from the contour $C$.

that clearly has poles at $k_0 = \mathrm{i}\omega_n + \mu$, for $n \in \mathbb{Z}$, with residues

$$\begin{aligned}\mathrm{Res}\left[n_{\mathrm{F}}(k_0-\mu)\right]_{k_0=\mathrm{i}\omega_n+\mu} &= \lim_{k_0\to\mathrm{i}\omega_n+\mu}\frac{(k_0-\mathrm{i}\omega_n-\mu)}{1+\mathrm{e}^{\beta(k_0-\mu)}}\\ &= \lim_{k_0\to\mathrm{i}\omega_n+\mu}\frac{(k_0-\mathrm{i}\omega_n-\mu)}{1+\mathrm{e}^{\mathrm{i}\beta\omega_n}\mathrm{e}^{\beta(k_0-\mathrm{i}\omega_n-\mu)}} = -\frac{1}{\beta},\end{aligned} \tag{3.9}$$

where the identity $\mathrm{e}^{\mathrm{i}\beta\omega_n} = -1$, valid for fermionic Matsubara frequencies, was applied.

Therefore, defining $\mathrm{i}q_4 + \mu \to k_0$, we calculate the contour integral depicted in figure 2, when the radius of the outer circular contour $\Gamma_R$ goes to infinity, $R \to \infty$, and the radius of the four contours $\gamma_\epsilon^{(\alpha)}$ goes to zero, $\varepsilon \to 0$

$$\begin{aligned}&\lim_{R\to\infty,\varepsilon\to 0}\oint_C \frac{N(Q,\mathrm{i}p_4,k_0)}{B^{EE}(Q,\mathrm{i}p_4,k_0)}n_{\mathrm{F}}(k_0-\mu)\frac{\mathrm{d}k_0}{2\pi\mathrm{i}}\\ &= -\sum_{\alpha=1,4}\mathrm{Res}\left[\frac{N(Q,\mathrm{i}p_4,k_0)}{B^{EE}(Q,\mathrm{i}p_4,k_0)}\right]_{k_0=k_0^{(\alpha)}} n_{\mathrm{F}}(k_0^{(\alpha)}-\mu)\\ &-\sum_{n\in Z}\frac{N(Q,\mathrm{i}p_4,\mathrm{i}\omega_n+\mu)}{B^{EE}(Q,\mathrm{i}p_4,\mathrm{i}\omega_n+\mu)}\mathrm{Res}\left[n_{\mathrm{F}}(k_0-\mu)\right]_{k_0=\mathrm{i}\omega_n+\mu} = 0.\end{aligned} \tag{3.10}$$

Using equation (3.9), we solve for the required Matsubara sum from the equation above,

$$\frac{1}{\beta}\sum_{n\in Z}\frac{N(Q,\mathrm{i}p_4,\mathrm{i}\omega_n+\mu)}{B^{EE}(Q,\mathrm{i}p_4,\mathrm{i}\omega_n+\mu)} = \sum_{\alpha=1,4}\mathrm{Res}\left[\frac{N(Q,\mathrm{i}p_4,k_0)}{B^{EE}(Q,\mathrm{i}p_4,k_0)}\right]_{k_0^{(\alpha)}} n_{\mathrm{F}}(k_0^{(\alpha)}-\mu). \tag{3.11}$$

Here, the poles are the roots of the denominator of the quartic polynomial, i.e. $B^{EE}(Q,\mathrm{i}p_4,k_0^{(\alpha)}) = 0$, for $\alpha = 1,\ldots,4$. Explicitly, one finds

$$
\begin{aligned}
k_0^{(1)} &= \frac{Q(Q+2mv_f)}{2m},\\
k_0^{(2)} &= \frac{Q(Q-2mv_f)}{2m},\\
k_0^{(3)} &= \frac{Q(Q+2mv_f)}{2m} - \mathrm{i}p_4,\\
k_0^{(4)} &= \frac{Q(Q-2mv_f)}{2m} - \mathrm{i}p_4.
\end{aligned}
\tag{3.12}
$$

By recalling that the external Matsubara frequency in the diagram is a Bosonic one, we have $p_4 = 2n\pi/\beta$, with $n \in \mathbb{Z}$, and hence $\mathrm{e}^{\mathrm{i}\beta p_4} = 1$. Using this simple identity, we find that

$$
n_{\mathrm{F}}(k_0^{(3)} - \mu) = n_{\mathrm{F}}(k_0^{(1)} - \mu), \quad n_{\mathrm{F}}(k_0^{(4)} - \mu) = n_{\mathrm{F}}(k_0^{(2)} - \mu). \tag{3.13}
$$

Using this, and calculating explicitly the residues, we finally obtain

$$
\begin{aligned}
\Pi_{11}^{E}(\mathrm{i}p_4, \mathbf{0}) = \frac{e^2}{4\pi}\int_0^\infty \mathrm{d}Q\, \frac{4v_f^3Q^2}{4v_f^2Q^2 - (\mathrm{i}\,p_4)^2}\left(n_{\mathrm{F}}\left[\frac{Q(Q-2mv_f)}{2m} - \mu\right]\right.\\
\left. - n_{\mathrm{F}}\left[\frac{Q(Q+2mv_f)}{2m} - \mu\right]\right).
\end{aligned}
\tag{3.14}
$$

From this expression, by analytic continuation to real frequency space $\mathrm{i}p_4 \to \omega + \mathrm{i}\epsilon$ we recover the retarded polarization tensor

$$
\Pi_{11}^{R}(\omega) = \Pi_{11}^{E}(\mathbf{0}, \mathrm{i}p_4 \to \omega + \mathrm{i}\epsilon). \tag{3.15}
$$

For this purpose, we write part of the integrand in equation (3.14) as follows

$$
\begin{aligned}
\frac{4v_f^3Q^2}{4v_f^2Q^2 - (\omega + \mathrm{i}\epsilon)^2} &= v_f^2Q\left[\frac{1}{2v_fQ - \omega - \mathrm{i}\epsilon} + \frac{1}{2v_fQ + \omega + \mathrm{i}\epsilon}\right]\\
&= \mathcal{P}\frac{4v_f^3Q^2}{4v_f^2Q^2 - \omega^2} + \mathrm{i}\pi v_f^2Q\left[\delta(2v_fQ - \omega) - \delta(2v_fQ + \omega)\right],
\end{aligned}
\tag{3.16}
$$

where $\mathcal{P}$ stands for the Cauchy principal value. Therefore, the real and imaginary parts of the retarded polarization tensor are given by the expressions

$$
\begin{aligned}
\Re e\,\Pi_{11}^{R}(\omega) = \frac{e^2}{4\pi}\mathcal{P}\int_0^\infty \mathrm{d}Q\, \frac{4v_f^3Q^2}{4v_f^2Q^2 - \omega^2}\left(n_{\mathrm{F}}\left[\frac{Q(Q-2mv_f)}{2m} - \mu\right]\right.\\
\left. - n_{\mathrm{F}}\left[\frac{Q(Q+2mv_f)}{2m} - \mu\right]\right)
\end{aligned}
\tag{3.17}
$$

$$
\begin{aligned}
\Im m\,\Pi_{11}^{R}(\omega) = \frac{e^2}{4}v_f^2\int_0^\infty \mathrm{d}Q\, Q\left[\delta(2v_fQ - \omega) - \delta(2v_fQ + \omega)\right]\\
\times\left(n_{\mathrm{F}}\left[\frac{Q(Q-2mv_f)}{2m} - \mu\right] - n_{\mathrm{F}}\left[\frac{Q(Q+2mv_f)}{2m} - \mu\right]\right).
\end{aligned}
\tag{3.18}
$$

Moreover, in order to remove unphysical vacuum contributions from the retarded polarization tensor, we define its regularized version as

$$
\Pi_{11,\,reg}^{R}(\omega) \equiv \Pi_{11}^{R}(\omega, T) - \Pi_{11}^{R}(0, T), \tag{3.19}
$$

where we have subtracted the (finite) limit of zero frequency of the right hand side of equation (3.17) (see appendix B). Note from the definitions above that, by construction, $\Im m\,\Pi^R_{11}(\omega=0,T)=0$, and hence no regularization is required for the imaginary part of the tensor. On the other hand, $\Re e\,\Pi_{11}(\omega=0,T)\neq 0$ in general, and hence the real part will be regularized as described in appendix. The expression for the real part cannot be reduced to a simple analytical expression, however one can still evaluate it in a low-temperature series through a generalization of Sommerfeld expansion (as shown in appendix B). On the other hand, the integral for the imaginary part can be evaluated to yield

$$\begin{aligned}\Im m\,\Pi^R_{11}(\omega) &= \frac{e^2}{16}\omega\,\mathrm{sgn}(\omega)\left(n_{\mathrm{F}}\left[\frac{\omega^2}{8mv_f^2}-\frac{\omega}{2}-\mu\right]-n_{\mathrm{F}}\left[\frac{\omega^2}{8mv_f^2}+\frac{\omega}{2}-\mu\right]\right)\\ &= \frac{e^2}{32}|\omega|\left(\tanh\left[\frac{\beta}{2}\left(\frac{\omega^2}{8mv_f^2}+\frac{\omega}{2}-\mu\right)\right]\right.\\ &\quad\left.-\tanh\left[\frac{\beta}{2}\left(\frac{\omega^2}{8mv_f^2}-\frac{\omega}{2}-\mu\right)\right]\right).\end{aligned}\tag{3.20}$$

From the expression above, the real part of the optical conductivity is given by

$$\begin{aligned}\Re e\,\sigma_{11}(\omega,T) &= 4\frac{\Im m\,\Pi^R_{11}(\omega)}{\omega}\\ &= \frac{e^2}{8\hbar}\,\mathrm{sgn}(\omega)\left(\tanh\left[\frac{\beta}{2}\left(\frac{\hbar^2\omega^2}{8mv_f^2}+\frac{\hbar\omega}{2}-\mu\right)\right]\right.\\ &\quad\left.-\tanh\left[\frac{\beta}{2}\left(\frac{\hbar^2\omega^2}{8mv_f^2}-\frac{\hbar\omega}{2}-\mu\right)\right]\right),\end{aligned}\tag{3.21}$$

where we have restored the $\hbar$ constant for normal I.S. units. The real part of the electrical conductivity, as a function of frequency and at different temperatures, is depicted in figures 3(a) and (b).

It is very interesting to analyze the zero-temperature limit ($\beta\to\infty$) of equation (3.21), that becomes (see appendix B for details)

$$\Re e\,\sigma_{11}(\omega,T\to 0)=\begin{cases}\frac{e^2}{4\hbar}, & \sqrt{1+\frac{2\mu}{mv_f^2}}-1<\frac{\hbar|\omega|}{2mv_f^2}<\sqrt{1+\frac{2\mu}{mv_f^2}}+1\\ 0, & \text{otherwise.}\end{cases}\tag{3.22}$$

It is seen from this result that the actual value of the conductivity at $T=0$ is $e^2/(4\hbar)$, independent of frequency and the parameter $m$ that captures the second nearest-neighbor interaction, in agreement with our previous calculation [31] and transparency experiments [3]. Interestingly though, there is however a hidden, non-analytic dependency through the domain of the step-wise function, that defines a region where the conductivity actually vanishes. It is instructive to compare our result, that includes the second nearest-neighbor interaction through the parameter $m$, with the more standard result that only involves first nearest-neighbors, a situation that can be recovered from our model in the limit $m\to\infty$. In this limit, from equation (3.21) we obtain

$$\begin{aligned}\Re e\,\sigma_{11}(\omega,T,m\to\infty) &= \frac{e^2}{8\hbar}\,\mathrm{sgn}(\omega)\left(\tanh\left[\frac{\beta}{2}\left(\frac{\hbar\omega}{2}-\mu\right)\right]\right.\\ &\quad\left.+\tanh\left[\frac{\beta}{2}\left(\frac{\hbar\omega}{2}+\mu\right)\right]\right).\end{aligned}\tag{3.23}$$

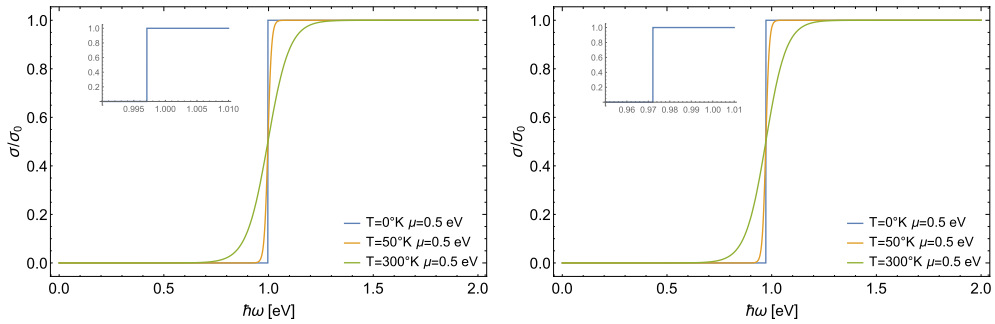


(a) $t' = 0.056\,eV$ (b) $t' = 0.56\,eV$

**Figure 3.** The real part of the conductivity, calculated from equation (3.21), for (a) $t' = 0.056$ eV, and (b) $t' = 0.56$ eV (see table 1), at constant chemical potential $\mu = 0.5$ eV, as a function of frequency, for different temperature values. On the inset of both figures is shown in detail the shift of the step from $2\mu = 1.0$ to $2\mu - \frac{\mu^2}{mv_f^2}$ as discussed in the main text.

This limit, as expected, matches the one reported in [41, 42]. We notice, however, that the effects of scattering by impurities [20, 21], many-body screening [19] or buckling of the lattice [18] will induce deviations from this behavior. Interestingly, equation (3.23) was also obtained as the main result in [43], starting from an expansion of the tight-binding dispersion relation, but later arguing that the second-nearest neighbor contribution is negligible. Here, through our exact result in equation (3.21), we explicitly show that such contribution is not negligible, but can be a measurable effect, as we later discuss in the Conclusions. As seen from equation (3.23), if the effect of second-nearest neighbors $t'$ is neglected ($m \to \infty$), the real part of the conductance displays a sigmoidal-shape centered at $\hbar\omega = 2\mu$. In contrast, when $t'$ is included as in our model equation (3.21), the center of the sigmoidal curve is shifted to $\hbar\omega = 2mv_f^2\left(\sqrt{1+\frac{2\mu}{mv_f^2}} - 1\right) \sim 2\mu - \frac{\mu^2}{mv_f^2}$, as displayed on the inset of figures 3(a) and (b). The predicted shift $\frac{\mu^2}{mv_f^2} = \left(\frac{9a^2\mu^2}{2\hbar^2 v_f^2}\right) t'$ is thus linear in $t'$. In the Conclusions section, we shall comment on the potential implications of this effect on the experimental determination of $t'$.

Also in the limit $m \to \infty$, the zero-temperature conductivity becomes

$$\Re e\,\sigma_{11}(\omega, 0, m \to \infty) = \frac{e^2}{8\hbar}\,\mathrm{sgn}(\omega)\,\{\,\mathrm{sgn}\,(\hbar\omega - 2\mu) + \,\mathrm{sgn}\,(\hbar\omega + 2\mu)\} \tag{3.24}$$

$$= \begin{cases} 0, & |\omega| < 2\mu/\hbar \\ \frac{e^2}{4\hbar}, & |\omega| > 2\mu/\hbar. \end{cases} \tag{3.25}$$

in agreement with [3, 42, 43].

Let us now turn to the imaginary part of the optical conductivity. The integral over $0 \leqslant Q < \infty$ can be expressed as an asymptotic expansion in negative powers of $\beta$, through a similar analysis as in the more standard Sommerfeld expansion (for details see appendix B). The real part of the retarded polarization tensor (see appendix B) is given by the expression

$$\begin{aligned}\Re e\,\Pi^R_{11,\mathrm{reg}}(\omega,T) &= \frac{e^2}{8\pi}\omega\mathcal{F}(\omega,\mu,m)+\beta^{-2}\frac{e^2\pi\omega^2}{24mv_f^2\left(1+\frac{2\mu}{mv_f^2}\right)^{3/2}}\\ &\times\left(\frac{\omega^2-8mv_f^2\left(3\mu+2mv_f^2\left(1+\sqrt{1+\frac{2\mu}{mv_f^2}}\right)\right)}{\left[\omega^2-8mv_f^2\left(\mu+mv_f^2\left(1+\sqrt{1+\frac{2\mu}{mv_f^2}}\right)\right)\right]^2}\right.\\ &\left.-\frac{\omega^2+8mv_f^2\left(-3\mu+2mv_f^2\left(-1+\sqrt{1+\frac{2\mu}{mv_f^2}}\right)\right)}{\left[\omega^2-8mv_f^2\left(\mu+mv_f^2\left(-1+\sqrt{1+\frac{2\mu}{mv_f^2}}\right)\right)\right]^2}\Theta\left[\frac{\mu}{mv_f^2}\right]\right)\\ &+O(\beta^{-3}).\end{aligned} \tag{3.26}$$

Therefore, the imaginary part of the optical conductivity is given by

$$\begin{aligned}\Im m\,\sigma_{11}(\omega) &= -4\frac{\Re e\,\Pi^R_{11,\mathrm{reg}}(\omega,T)}{\omega}\\ &= -\frac{e^2}{2\pi\hbar}\mathcal{F}(\omega,\mu,m)-(k_{\mathrm{B}}T)^2\frac{e^2\pi\omega}{6mv_f^2\left(1+\frac{2\mu}{mv_f^2}\right)^{3/2}}\\ &\times\left(\frac{\hbar^2\omega^2-8mv_f^2\left(3\mu+2mv_f^2\left(1+\sqrt{1+\frac{2\mu}{mv_f^2}}\right)\right)}{\left[\hbar^2\omega^2-8mv_f^2\left(\mu+mv_f^2\left(1+\sqrt{1+\frac{2\mu}{mv_f^2}}\right)\right)\right]^2}\right.\\ &\left.-\frac{\hbar^2\omega^2+8mv_f^2\left(-3\mu+2mv_f^2\left(-1+\sqrt{1+\frac{2\mu}{mv_f^2}}\right)\right)}{\left[\hbar^2\omega^2-8mv_f^2\left(\mu+mv_f^2\left(-1+\sqrt{1+\frac{2\mu}{mv_f^2}}\right)\right)\right]^2}\Theta\left[\frac{\mu}{mv_f^2}\right]\right)\\ &+O(\beta^{-3}),\end{aligned} \tag{3.27}$$

where we have restored the $\hbar$ constant for I.S. units, and we defined the function

$$\mathcal{F}(\omega,\mu,m)=\begin{cases}\operatorname{arctanh}\left[\frac{\hbar\omega}{2mv_f^2\left(\sqrt{1+\frac{2\mu}{mv_f^2}}-1\right)}\right]-\operatorname{arctanh}\left[\frac{\hbar\omega}{2mv_f^2\left(\sqrt{1+\frac{2\mu}{mv_f^2}}+1\right)}\right],\\ \qquad\text{if}\quad 0<\hbar\omega<2mv_f^2\left(\sqrt{1+\frac{2\mu}{mv_f^2}}-1\right).\\ \frac{1}{2}\ln\left[\frac{\left(\sqrt{1+\frac{2\mu}{mv_f^2}}+1-\frac{\hbar\omega}{2mv_f^2}\right)}{\left(\sqrt{1+\frac{2\mu}{mv_f^2}}+1+\frac{\hbar\omega}{2mv_f^2}\right)}\frac{\left(\sqrt{1+\frac{2\mu}{mv_f^2}}-1+\frac{\hbar\omega}{2mv_f^2}\right)}{\left(\frac{\hbar\omega}{2mv_f^2}-\sqrt{1+\frac{2\mu}{mv_f^2}}+1\right)}\right],\\ \qquad\text{if}\quad \sqrt{1+\frac{2\mu}{mv_f^2}}-1<\frac{\hbar\omega}{2mv_f^2}<\sqrt{1+\frac{2\mu}{mv_f^2}}+1.\\ \operatorname{arctanh}\left[\frac{2mv_f^2\left(\sqrt{1+\frac{2\mu}{mv_f^2}}-1\right)}{\hbar\omega}\right]-\operatorname{arctanh}\left[\frac{2mv_f^2\left(\sqrt{1+\frac{2\mu}{mv_f^2}}+1\right)}{\hbar\omega}\right],\\ \qquad\text{if}\quad \hbar\omega>2mv_f^2\left(\sqrt{1+\frac{2\mu}{mv_f^2}}+1\right).\end{cases} \tag{3.28}$$

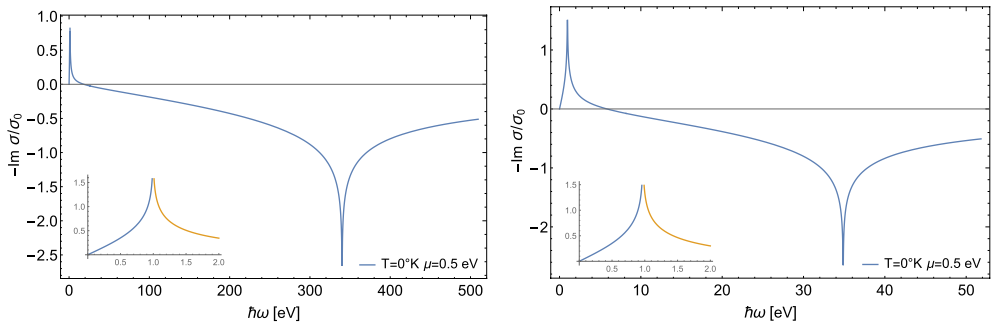


(a) $t' = 0.056\,eV$ (b) $t' = 0.56\,eV$

**Figure 4.** The imaginary part of the electrical conductance, for (a) $t' = 0.056$ eV, and (b) $t' = 0.56$ eV (see table 1), at constant chemical potential $\mu = 0.5$ eV, as a function of frequency, at zero temperature. The finite temperature dependence is very weak (as seen in equation (3.27) and cannot be appreciated at the scale of the plot. The inset shows with higher resolution the region near the first peak.

The imaginary part of the optical conductivity, expressed in our model by equation (3.27), displays two separate resonances (see figures 4(a) and (b)), the first at $\hbar\omega = 2mv_f^2\left(\sqrt{1+\frac{2\mu}{mv_f^2}}-1\right) \sim 2\mu - \frac{\mu^2}{mv_f^2}$, and the second at $\hbar\omega = 2mv_f^2\left(\sqrt{1+\frac{2\mu}{mv_f^2}}+1\right) \sim 2mv_f^2$. The first one reproduces, in the limit $m \to \infty$, results reported in the literature for the conventional model with only first-to-nearest neighbor approximation [3, 42], with a small shift $\sim -\frac{\mu^2}{mv_f^2}$ in the position of the peak. The second peak, which is a unique feature of the model, is located at an extremely large frequency, and in practice has no physical consequences.

## 4. Conclusions

Throughout this article, we have discussed the effect of including the next-to-nearest neighbors hopping $t'$, through the 'mass' parameter $m = 2\hbar^2/(9t'a^2)$ in the dispersion relation [2], on the optical conductivity of single-layer graphene. Our analysis is based on the continuum representation of the model via an effective field theory [31], by extending our previous results at zero temperature [31] to the finite chemical potential and finte temperature scenario, equations (3.21) and (3.27). As expected, our analytical calculation recovers the universal value $\Re e\,\sigma \to e^2/(4\hbar)$ in the limit of zero temperature, equation (3.22), but however reveals a non-trivial and non-analytic dependence on the second-nearest neighbor hopping $t'$ through the ratio $\mu/(mv_f^2)$ in the frequency domain. Remarkably, our analytical equation (3.21) for the frequency-dependent real part of the optical conductivity at finite temperature and chemical potential, in the limit $m \to \infty$ ($t' \to 0$) reduces to equation (3.23), that exactly reproduces previous results reported in the literature [3, 21, 42] for the conventional first-nearest neighbor approximation. More importantly, and this is the main novelty of our work, our equation (3.21) generalizes this result to reveal the effect of including the next-to-nearest neighbor hopping $t'$ into the dispersion relation. In particular, we notice that, when $t'$ is neglected as in the conventional case, the real part of the conductivity presents a sharp step (at zero

temperature) or a sigmoidal shape (at finite temperature) exactly centered at $\hbar\omega = 2\mu$ [3, 21, 42] (see for instance equation (3.23)). In contrast, when $t'$ is included as in our model, the step is shifted to $\hbar\omega = 2mv_f^2\left(\sqrt{1+\frac{2\mu}{mv_f^2}}-1\right) \sim 2\mu - \frac{\mu^2}{mv_f^2}$. The predicted shift $\frac{\mu^2}{mv_f^2} = \left(\frac{9a^2\mu^2}{2\hbar^2 v_f^2}\right)t'$ is thus linear in $t'$. This effect is particularly interesting since, as shown in the existing literature [30], there seems to be a large uncertainty on the exact value for the second-nearest neighbors hopping in graphene, $0.056\ \text{eV} < t' < 0.56\ \text{eV}$ (see table 1). The order of magnitude of this shift can be estimated from the parameters in table 1, where the reported range of $t'$ implies that $7\,\text{eV} < mv_f^2 < 70\,\text{eV}$, and hence for a chemical potential of $\mu \sim 0.5\,\text{eV}$, we have $3.6\,\text{meV} < \frac{\mu^2}{mv_f^2} < 36\,\text{meV}$, which is a value accessible to be detected in transport experiments. Our result therefore suggests that an experimental characterization of the frequency-dependence of the real part of the optical conductivity, at finite chemical potential (to be adjusted, for instance, with a gate potential) could provide an accurate and direct experimental measurement of $t'$, to be compared with the broad estimations obtained so far from *ab initio* calculations [44] or cyclotron resonance experiments [45].

## Acknowledgments

H F thanks ANPCyT, CONICET and UNLP, Argentina, for partial support through grants PICT-2014-2304, PIP 2015-688 and Proy. Nro. 11/X748, respectively. H F also acknowledges PUC for its kind hospitality. E M acknowledges support from FONDECYT (Chile) under Grant No. 1190361. M L acknowledges support from FONDECYT (Chile) under Grants No. 1170107 and No. 1190192, and Conicyt PIA/Basal Fb0821 (Chile). R Z would like to thank support from CONICYT FONDECYT Iniciación under Grant No. 11160234.

## Appendix A. Zero temperature limit of $\Re e\,\sigma_{11}(\omega, T)$

Let us start from equation (3.21) (in natural units $\hbar = 1$), and consider the limit $T \to 0$ ($\beta \to \infty$),

$$\Re e\,\sigma_{11}(\omega, T=0) = \frac{e^2}{8}\,\text{sgn}(\omega)\left(\text{sgn}\left[\frac{\omega^2}{4mv_f^2}+\omega-2\mu\right] - \text{sgn}\left[\frac{\omega^2}{4mv_f^2}-\omega-2\mu\right]\right). \tag{A.1}$$

Clearly, the difference between the $\text{sgn}(z)$ functions is either $\pm 2$ or 0. In order to analyze the different cases, let us define the two quadratic functions

$$\begin{aligned} y_1(\omega) &= \frac{\omega^2}{4mv_f^2}+\omega-2\mu = (\omega-\omega_+^{(1)})(\omega-\omega_-^{(1)}),\\ y_2(\omega) &= \frac{\omega^2}{4mv_f^2}-\omega-2\mu = (\omega-\omega_+^{(2)})(\omega-\omega_-^{(2)}), \end{aligned} \tag{A.2}$$

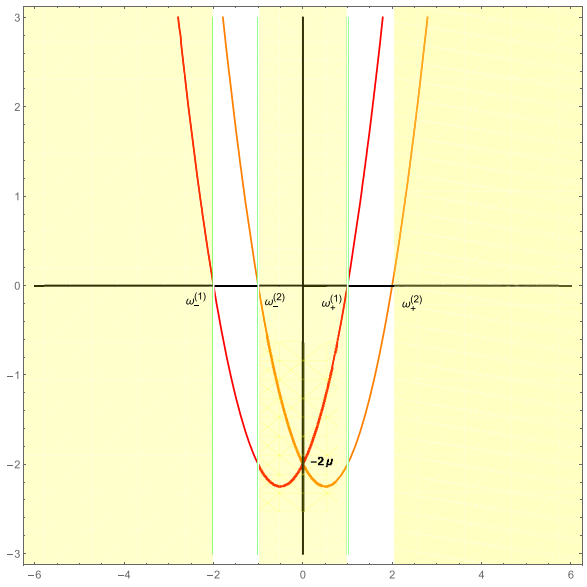


**Figure A1.** Sketch of the locus of the roots in equation (A.3). The regions in white represent the frequency range where, at zero temperature and finite chemical potential, the real part of the optical conductivity does not vanish, as seen in equation (A.5).

where roots are given by

$$\begin{aligned}\omega_{\pm}^{(1)} &= -2mv_f^2 \pm 2mv_f^2\sqrt{1+\frac{2\mu}{mv_f^2}},\\ \omega_{\pm}^{(2)} &= 2mv_f^2 \pm 2mv_f^2\sqrt{1+\frac{2\mu}{mv_f^2}}.\end{aligned} \tag{A.3}$$

On the other hand, the two parabolas intersect at $\omega = 0$, with the common value $y_1(0) = y_2(0) = -2\mu$. A graphical representation of the roots and intercept is displayed in figure A1. Moreover, we remark that equation (A.1) can be written as

$$\begin{aligned}\Re e\,\sigma_{11}(\omega, T=0) &= \frac{e^2}{8}\,\mathrm{sgn}(\omega)\,(\,\mathrm{sgn}(y_1) - \,\mathrm{sgn}(y_2))\\ &= \frac{e^2}{4}\begin{cases}\mathrm{sgn}(\omega), & y_1(\omega)>0,\ y_2(\omega)<0\\ -\mathrm{sgn}(\omega), & y_1(\omega)<0,\ y_2(\omega)>0\\ 0, & \text{otherwise.}\end{cases}\end{aligned} \tag{A.4}$$

The condition $y_1(\omega) > 0$ and $y_2(\omega) < 0$ is satisfied for $-2mv_f^2 + 2mv_f^2\sqrt{1+\frac{2\mu}{mv_f^2}} < \omega < 2mv_f^2 + 2mv_f^2\sqrt{1+\frac{2\mu}{mv_f^2}}$, where $\mathrm{sgn}(\omega) = 1$. On the other hand, the condition $y_1(\omega) < 0$ and $y_2(\omega) > 0$ is satisfied for $-2mv_f^2 - 2mv_f^2\sqrt{1+\frac{2\mu}{mv_f^2}} < \omega < 2mv_f^2 - 2mv_f^2\sqrt{1+\frac{2\mu}{mv_f^2}}$, where $\mathrm{sgn}(\omega) = -1$. Taking this into account, we arrive at the final expression

$$\Re e\,\sigma_{11}(\omega, T\to 0) = \begin{cases}\frac{e^2}{4\hbar}, & \sqrt{1+\frac{2\mu}{mv_f^2}} - 1 < \frac{\hbar|\omega|}{2mv_f^2} < \sqrt{1+\frac{2\mu}{mv_f^2}} + 1\\ 0, & \text{otherwise}\end{cases} \tag{A.5}$$

where we have restored the $\hbar$ constant for I.S. units.

## Appendix B. Low temperature expansion for $\Re e\,\Pi^R_{11}(\omega)$

Let us consider the integral representing the real part of the retarded polarization tensor

$$\Re e\,\Pi^R_{11}(\omega) = \frac{e^2}{4\pi}\mathcal{P}\int_0^\infty \mathrm{d}Q\,\frac{4v_f^3Q^2}{4v_f^2Q^2-\omega^2}\left(n_{\mathrm{F}}\left[\frac{Q(Q-2mv_f)}{2m}-\mu\right]\right.$$
$$\left.-n_{\mathrm{F}}\left[\frac{Q(Q+2mv_f)}{2m}-\mu\right]\right), \tag{B.1}$$

where $\mathcal{P}$ stands for Cauchy's principal value.

It is convenient to express the integral defining the polarization tensor in dimensionless variables, i.e.

$$x = Q/(mv_f),\quad \Omega = \omega/(2mv_f^2),\quad \bar\beta = mv_f^2\beta/2,\quad \gamma = 2\mu/(mv_f^2). \tag{B.2}$$

Hence, we have

$$\Re e\,\Pi^R_{11}(\omega) = \frac{e^2}{8\pi}mv_f^2\mathcal{P}\int_0^\infty \mathrm{d}x\,\left[\frac{x}{x+\Omega}+\frac{x}{x-\Omega}\right]\left[\bar n_{\mathrm{F}}(x^2-2x-\gamma)\right.$$
$$\left.-\bar n_{\mathrm{F}}(x^2+2x-\gamma)\right], \tag{B.3}$$

with the Fermi distributions at the dimensionless $\bar\beta$,

$$\bar n_{\mathrm{F}}(z) = \left(1+\mathrm{e}^{\bar\beta z}\right)^{-1}. \tag{B.4}$$

As discussed in the main text, in order to remove spurious unphysical contributions arising from the vacuum, we regularize the retarded polarization tensor according to the expression

$$\Re e\,\Pi^R_{11,\mathrm{reg}}(\omega,T) \equiv \Re e\,\Pi^R_{11}(\omega,T) - \Re e\,\Pi^R_{11}(0,T), \tag{B.5}$$

where we have subtracted the (finite[8]) zero frequency limit of the right hand side of equation (B.3).

It is interesting first to analyze the $T\to 0$ limit of the regularized polarization tensor. From the expression for the Fermi functions, it is clear that $\bar n_{\mathrm{F}}(z)\to\Theta(-z)$ as $\bar\beta\to\infty$ $(T\to 0)$. Therefore, we have

$$\Re e\,\Pi^R_{11,\mathrm{reg}}(\omega,T\to 0) = \frac{e^2}{4\pi}mv_f^2\Omega^2\mathcal{P}\int_0^\infty \mathrm{d}x\,\frac{1}{x^2-\Omega^2}\left[\Theta(x^2+2x-\gamma)\right.$$
$$\left.-\Theta(x^2-2x-\gamma)\right],$$
$$= \frac{e^2}{4\pi}mv_f^2\Omega^2\mathcal{P}\int_{x_+^{(1)}}^{x_+^{(2)}}\frac{\mathrm{d}x}{x^2-\Omega^2}, \tag{B.6}$$

[8] Indeed, the term with the factor $x/(x+\Omega)$ gives rise to a uniformly convergent integral for $\Omega\geqslant 0$, while the term with the $x/(x-\Omega)$ factor gives a finite (and identical to the previous one) contribution in this limit, by virtue of the principal value operator.

where $x_+^{(1)}=\sqrt{1+\gamma}-1$ and $x_+^{(2)}=\sqrt{1+\gamma}+1$ are the positive roots of the quadratic polynomials $y_1(x)=x^2+2x-\gamma$ and $y_2(x)=x^2-2x-\gamma$, respectively. The principal value integral must be calculated separately in three frequency intervals, giving the results

$$\mathcal{P}\int_{x_+^{(1)}}^{x_+^{(2)}}\frac{\mathrm{d}x}{x^2-\Omega^2}=\begin{cases}\frac{1}{\Omega}\left[\operatorname{arctanh}(\Omega/x_+^{(1)})-\operatorname{arctanh}(\Omega/x_+^{(2)})\right], & 0<\Omega<x_+^{(1)}\\ \frac{1}{2\Omega}\ln\left[\frac{x_+^{(2)}-\Omega}{x_+^{(2)}+\Omega}\frac{x_+^{(1)}+\Omega}{\Omega-x_+^{(1)}}\right], & x_+^{(1)}<\Omega<x_+^{(2)}\\ \frac{1}{\Omega}\left[\operatorname{arctanh}(x_+^{(1)}/\Omega)-\operatorname{arctanh}(x_+^{(2)}/\Omega)\right], & \Omega>x_+^{(2)}.\end{cases} \tag{B.7}$$

Therefore, we have the analytical expression

$$\Re e\,\Pi_{11,\mathrm{reg}}^R(\omega,T\to 0)=\frac{e^2}{8\pi}\omega\mathcal{F}(\omega,\mu,m) \tag{B.8}$$

where we have defined the function

$$\mathcal{F}(\omega,\mu,m)=\begin{cases}\operatorname{arctanh}\left[\frac{\omega}{2mv_f^2\left(\sqrt{1+\frac{2\mu}{mv_f^2}}-1\right)}\right]-\operatorname{arctanh}\left[\frac{\omega}{2mv_f^2\left(\sqrt{1+\frac{2\mu}{mv_f^2}}+1\right)}\right],\\ \qquad\text{if}\ \ 0<\omega<2mv_f^2\left(\sqrt{1+\frac{2\mu}{mv_f^2}}-1\right).\\ \frac{1}{2}\ln\left[\frac{\left(\sqrt{1+\frac{2\mu}{mv_f^2}}+1-\frac{\omega}{2mv_f^2}\right)}{\left(\sqrt{1+\frac{2\mu}{mv_f^2}}+1+\frac{\omega}{2mv_f^2}\right)}\frac{\left(\sqrt{1+\frac{2\mu}{mv_f^2}}-1+\frac{\omega}{2mv_f^2}\right)}{\left(\frac{\omega}{2mv_f^2}-\sqrt{1+\frac{2\mu}{mv_f^2}}+1\right)}\right],\\ \qquad\text{if}\ \ \sqrt{1+\frac{2\mu}{mv_f^2}}-1<\frac{\omega}{2mv_f^2}<\sqrt{1+\frac{2\mu}{mv_f^2}}+1.\\ \operatorname{arctanh}\left[\frac{2mv_f^2\left(\sqrt{1+\frac{2\mu}{mv_f^2}}-1\right)}{\omega}\right]-\operatorname{arctanh}\left[\frac{2mv_f^2\left(\sqrt{1+\frac{2\mu}{mv_f^2}}+1\right)}{\omega}\right],\\ \qquad\text{if}\ \ \omega>2mv_f^2\left(\sqrt{1+\frac{2\mu}{mv_f^2}}+1\right).\end{cases} \tag{B.9}$$

For the finite temperature contribution, we obtain

$$\begin{aligned}\Re e\,\Pi_{11,\mathrm{reg}}^R(\omega,T)&=\Re e\,\Pi_{11,\mathrm{reg}}^R(\omega,T\to 0)\\ &\quad+\frac{e^2}{2\pi}mv_f^2\left(\Pi_1(\omega)-\Pi_2(\omega)-\Pi_1(0)+\Pi_2(0)\right),\end{aligned} \tag{B.10}$$

where

$$\begin{aligned}\Pi_1(\omega)&=2\sum_{k=0}^{N}\beta^{-2k-2}\left(1-2^{-2k-1}\right)\zeta(2k+2)F_+^{(2k+1)}(0)\\ &\quad+\delta_\gamma\left[\sum_{k=1}^{2N}\beta^{-k-1}\left(1-2^{-k}\right)(-1)^k\zeta(k+1)F_-^{(k)}(0)+\beta^{-1}F_-(0)\log(2)\right]_{\gamma\to 0}\end{aligned} \tag{B.11}$$

$$\Pi_2(\omega) = 2\theta(\gamma)\sum_{k=0}^{N}\beta^{-2k-2}\left(1-2^{-2k-1}\right)\zeta(2k+2)G_+^{(2k+1)}(0)$$
$$+\,\delta_\gamma\left[\sum_{k=1}^{2N}\beta^{-k-1}\left(1-2^{-k}\right)(-1)^k\zeta(k+1)G_+^{(k)}(0)+\beta^{-1}G_+(0)\log(2)\right]_{\gamma\to 0}. \tag{B.12}$$

In these expressions, we have defined the auxiliary functions obtained from the roots of the quadratic equations $x^2 \pm 2x - \gamma = z$, corresponding to

$$\begin{aligned} x_\pm^{(1)}(z) &= 1 \pm \sqrt{1+\gamma+z},\\ x_\pm^{(2)}(z) &= -1 \pm \sqrt{1+\gamma+z}, \end{aligned} \tag{B.13}$$

and the corresponding implicit functions

$$\begin{aligned} F_\pm(z) &= \frac{f[x_\pm^{(1)}(z)]}{2(x_\pm^{(1)}(z)-1)}\\ G_\pm(z) &= \frac{f[x_\pm^{(2)}(z)]}{2(x_\pm^{(2)}(z)+1)}, \end{aligned} \tag{B.14}$$

where we defined the function

$$f(x) = \frac{x^2}{x^2-\Omega^2}. \tag{B.15}$$

Similarly, in the above expansions we defined the derivatives of these implicit functions with respect to $z$, as

$$F_\pm^{(k)}(0) = \left.\frac{\mathrm{d}^k}{\mathrm{d}z^k}F_\pm(z)\right|_{z=0}, \quad G_\pm^{(k)}(0) = \left.\frac{\mathrm{d}^k}{\mathrm{d}z^k}G_\pm(z)\right|_{z=0}. \tag{B.16}$$

The explicit expression for finite temperature corrections up to $O(\beta^{-3})$ is

$$\begin{aligned} \Re e\,\Pi^R_{11,\mathrm{reg}}(\omega,T) = {}& \frac{e^2}{8\pi}\omega\mathcal{F}(\omega,\mu,m) + \beta^{-2}\frac{e^2\pi\omega^2}{24mv_f^2\left(1+\frac{2\mu}{mv_f^2}\right)^{3/2}}\\ &\times\left(\frac{\omega^2-8mv_f^2\left(3\mu+2mv_f^2\left(1+\sqrt{1+\frac{2\mu}{mv_f^2}}\right)\right)}{\left[\omega^2-8mv_f^2\left(\mu+mv_f^2\left(1+\sqrt{1+\frac{2\mu}{mv_f^2}}\right)\right)\right]^2}\right.\\ &\left.-\frac{\omega^2+8mv_f^2\left(-3\mu+2mv_f^2\left(-1+\sqrt{1+\frac{2\mu}{mv_f^2}}\right)\right)}{\left[\omega^2-8mv_f^2\left(\mu+mv_f^2\left(-1+\sqrt{1+\frac{2\mu}{mv_f^2}}\right)\right)\right]^2}\Theta\left[\frac{\mu}{mv_f^2}\right]\right)\\ &+O(\beta^{-3}). \end{aligned} \tag{B.17}$$

Here, we have defined the Heaviside Theta function as

$$\theta(x) = \begin{cases} 1, & x>0\\ 0, & x\leqslant 0. \end{cases} \tag{B.18}$$

## ORCID iDs

Horacio Falomir https://orcid.org/0000-0001-8188-1062
Enrique Muñoz https://orcid.org/0000-0003-4457-0817

## References

[1] Wallace P R 1947 *Phys. Rev.* **71** 622
[2] Falomir H, Gamboa J, Loewe M and Nieto M 2012 *J. Phys. A: Math. Theor.* **45** 135308
[3] Nair R R, Blake P, Grigorenko A N, Novoselov K S, Booth T J, Stauber T, Peres N M R and Geim A K 2008 *Science* **320** 1308
[4] Wassei J K and Kaner R B 2010 *Mater. Today* **13** 52
[5] Ma X and Zhang H 2013 *Nanoscale Ress. Lett.* **8** 440
[6] Mak K-F, Sfeir M-Y, Misewich J A and Heinz T F 2010 *Proc. Natl Acad. Sci.* **107** 14999
[7] Zhu S-E, Yuan S and Janssen G C A M 2014 *Europhys. Lett.* **108** 17007
[8] Fialkovsky I V and Vassilevich D V 2012 *Eur. Phys. J.* B **85** 384
[9] Beneventano C G, Fialkovsky I V, Santangelo E M and Vassilevich D V 2014 *Eur. Phys. J.* B **87** 50
[10] Fialkovsky I V and Vassilevich D V 2016 *Mod. Phys. Lett.* A **31** 1630047
[11] Fialkovsky I V and Vassilevich D V 2012 *Int. J. Mod. Phys. Conf. Ser.* 14 88
[12] Fialkovsky I V and Vassilevich D V 2012 *Int. J. Mod. Phys.* A **27** 1260007
[13] Fialkovsky I V and Vassilevich D V 2009 *J. Phys. A: Math. Theor.* **42** 442001
[14] Valenzuela S, Hernández-Ortiz D, Loewe M and Raya A 2015 *J. Phys. A: Math. Theor.* **48** 065402
[15] Hernández-Ortiz S, Valenzuela D, Raya A and Sánchez-Madrigal S 2016 *Int. J. Mod. Phys.* B **30** 1650084
[16] Merthe D J and Kresin V V 2016 *Phys. Rev.* B **94** 205439
[17] Das Sarma S, Adam S, Hwang E H and Rossi E 2011 *Rev. Mod. Phys.* **83** 407
[18] Iurov A, Gumbs G and Huang D 2018 *Phys. Rev.* B **98** 075414
[19] Iurov A, Gumbs G and Huang D 2017 *J. Phys.: Condens. Matter* **29** 135602
[20] Hwang E H and Das Sarma S 2009 *Phys. Rev.* B **79** 165404
[21] Falkovsky I V and Varlamov A A 2007 *Eur. Phys. J.* B **56** 281
[22] Kotov V N, Uchoa B, Pereira V M, Guinea F and Castro Neto A H 2012 *Rev. Mod. Phys.* **84** 1067
[23] Muñoz E 2016 *Graphene Science Handbook Vol. 3: Electrical and Optical Properties* (London: Taylor and Francis)
[24] Hwang E H and Das Sarma S 2008 *Phys. Rev.* B **77** 115449
[25] Tse W-K and Das Sarma S 2007 *Phys. Rev. Lett.* **99** 236802
[26] Muñoz E 2012 *J. Phys.: Condens. Matter* **24** 195302
[27] Kubakaddi S S 2009 *Phys. Rev.* B **79** 075417
[28] Peres N M R 2010 *Rev. Mod. Phys.* **82** 2673
[29] Ando T 2006 *J. Phys. Soc. Japan* **75** 096001
[30] Castro Neto A-H, Guinea F, Peres N M R, Novoselov K S and Geim A K 2009 *Rev. Mod. Phys.* **81** 109
[31] Falomir H, Loewe M, Muñoz E and Raya A 2018 *Phys. Rev.* B **98** 195430
[32] Luo J 2013 (arXiv:1303.7290)
[33] Kubo R, Toda M and Hashitume N 1991 *Statistical Physics* II (New York: Springer)
[34] Wen X-G 2010 *Quantum Field Theory of Many-Body Systems* (Oxford: Oxford University Press)
[35] Stefanucci G and van Leeuwen R 2013 *Nonequilibrium Many-Body Theory of Quantum Systems* (Cambridge: Cambridge University Press)
[36] Rammer J 2007 *Quantum Field Theory of Non-Equilibrium States* (Cambridge: Cambridge University Press)
[37] Altland A and Simons B 2010 *Condensed Matter Field Theory* (Cambridge: Cambridge University Press)
[38] Kamenev A 2011 *Field Theory of Non-Equilibrium Systems* (Cambridge: Cambridge University Press)
[39] Muñoz E, Bolech C J and Kirchner S 2013 *Phys. Rev. Lett.* **110** 016601
[40] Merker L, Kirchner S, Muñoz E and Costi T-A 2013 *Phys. Rev.* B **87** 165132

[41] Falkovsky L A and Pershoguba S S 2007 *Phys. Rev.* B **76** 153410
[42] Kuzmenko A B, van Heumen E, Carbone F and van der Marel D 2008 *Phys. Rev. Lett.* **100** 117401
[43] Stauber T, Peres N M R and Geim A K 2008 *Phys. Rev.* B **78** 085432
[44] Reich S, Maultzsch J, Thomsen C and Ordejón P 2002 *Phys. Rev.* B **66** 035412
[45] Deacon R S, Chuang K-C, Nicholas R J, Novoselov K S and Geim A K 2007 *Phys. Rev.* B **76** 081406